Asian Journal of Chemistry; Vol. 38, No. 3 (2026), 767-773
ASIAN JOURNAL OF CHEMISTRY
https://doi.org/10.14233/ajchem.2026.35345

Design, Synthesis and Anticancer Evaluation of Imidazo Pyridine Fused Thiazole Derivatives

SHERIN ABDUL and VELMURUGAN VADIVEL*,

Department of Pharmaceutical Chemistry Faculty of Medicine and Health Sciences, SRM Institute of Science and Technology, SRM College of Pharmacy, Kattankulathur-603203, India

*Corresponding author: E-mail: velmuruv@srmist.edu.in

Received: 28 November 2025 *Accepted*: 3 February 2026 *Published online*: 6 March 2026 AJC-22296

Breast cancer remains a major global health burden, driving the need for new therapeutic agents with improved efficacy and safety. In this study, a novel library of imidazopyridine-fused thiazole derivatives (**4a-j**) was rationally designed, synthesised and tested for anticancer efficacy using the MCF-7 breast cancer cell line. The design combined two well-established pharmacophores imidazopyridine and thiazole to enhance cytotoxic potential through synergistic structural features. The synthesis followed a four-step pathway starting from 2-(6-methyl-2-(*p*-tolyl)imidazopyridin-3-yl) acetonitrile. Base hydrolysis generated acetic acid (**1**), which was coupled with ethyl 2-aminothiazole-5-carboxylate using TBTU to form intermediate (**2**). Subsequent hydrolysis yielded acid (**3**), which underwent EDAC/HOBt-mediated amide coupling with various benzylamines to afford derivatives **4a-j**. All the compounds were characterized by IR, ^{1}H and ^{13}C NMR and mass spectrometry. Molecular docking on human Akt kinase (PDB: 7NH5) showed favourable binding across the series. Compound **4f** showed the strongest predicted Akt affinity (-10.024 kcal/mol), followed by **4i**, **4g** and **4d**, though all remained weaker than the reference inhibitor borussertib (-12.63 kcal/mol). *In vitro* MTT assays revealed significant cytotoxicity for compounds **4i**, **4e** and **4b**, with IC_{50} values of 35.85, 60.84 and 64.69 μM, respectively. Among them, compound **4i** emerged as the most promising lead for further optimisation and mechanistic investigation.

Keywords: Imidazopyridine, Thiazole, Breast cancer, Akt inhibition.

INTRODUCTION

Imidazopyridines are fused bicyclic nitrogen-containing heterocycles composed of an imidazole ring condensed with a pyridine nucleus, resulting in a rigid, planar and π-conjugated framework [1]. The presence of multiple ring nitrogens confers distinct electronic characteristics including hydrogen-bond donor–acceptor capacity and favourable charge distribution, which are critical for molecular recognition in enzyme active sites [2].

Structurally, the imidazopyridine core closely resembles the purine scaffold, enabling effective accommodation within ATP-binding pockets of kinases and other nucleotide dependent proteins [3]. From a synthetic chemistry perspective, this scaffold supports extensive substitution at multiple positions, allowing systematic modulation of steric, electronic and lipophilic properties during structure activity relationship (SAR) optimisation [4].

Thiazoles are five-membered aromatic heterocycles containing sulfur and nitrogen heteroatoms, imparting high polarizability and aromatic stability to the ring system [5]. The sulphur atom enhances π–π stacking and van der Waals interactions, while the ring nitrogen functions as a hydrogen-bond acceptor, together facilitating strong and selective ligand-protein interactions [6]. Chemically, thiazoles are versatile and robust motifs that tolerate a wide range of synthetic transformations, making them highly suitable for medicinal chemistry programs [7]. Their frequent occurrence among bioactive molecules and approved drugs underscores their chemical and pharmaceutical relevance [8].

Due to these complementary structural features, both imidazopyridines and thiazoles are widely recognised as privileged scaffolds in drug discovery [9]. Large-scale analyses of FDA-approved drugs reveal a high prevalence of nitrogen- and sulphur-containing heterocycles, particularly in anticancer and kinase-inhibitor classes [10]. The capacity of these scaffolds to engage in multiple non-covalent interactions, including hydrogen bonding, aromatic stacking and hydrophobic contacts, contributes to their broad biological applicability [11].

From a pharmacological standpoint, imidazopyridine derivatives have demonstrated diverse biological activities, including antimicrobial, anti-inflammatory, antiviral and anticancer effects [12]. In oncology research, imidazopyridines have gained prominence due to their ability to inhibit key signalling proteins such as PI3K, Akt, EGFR and cyclin-dependent kinases [13]. Several imidazopyridine-based compounds have shown significant antiproliferative activity against breast cancer cell lines through modulation of oncogenic signalling pathways and induction of apoptosis [14].

Notably, the imidazopyridine derivative was reported to suppress breast cancer progression by interfering with Wnt/β-catenin signaling, further validating this scaffold as a promising anticancer pharmacophore [15]. Similarly, thiazole-containing compounds have attracted considerable attention in anticancer drug development [16]. Recent studies demonstrate that thiazole derivatives can disrupt cancer-associated pathways, including PI3K/Akt/mTOR and NF-κB signalling, leading to inhibition of tumor cell growth and survival [17]. Several small-molecule Akt inhibitors such as capivasertib, ipatasertib and perifosine have entered clinical trials, showing promising efficacy in advanced and triple-negative breast cancer.

Incorporation of thiazole moieties has also been associated with improved pharmacokinetic behaviour, metabolic stability and target selectivity in anticancer lead compounds [18]. The rational hybridisation of imidazopyridine and thiazole frameworks represents an effective medicinal-chemistry strategy to enhance binding affinity and biological potency [19]. Such hybrid molecules can exploit the ATP-mimetic characteristics of imidazopyridines alongside the electron-rich and polarizable nature of thiazoles, enabling stronger and more selective interactions with kinase active sites [20]. Given the central role of Akt signaling in breast cancer progression and therapeutic resistance, this hybrid scaffold design offers a compelling approach for the development of next-generation anticancer agents. Thus, the present study focuses on the structure-guided design and multistep synthesis of imidazopyridine-fused thiazole derivatives, followed by molecular docking, Akt active-site interaction analysis and *in vitro* anticancer evaluation to identify optimised scaffolds capable of modulating Akt-driven oncogenic signalling in breast cancer.

EXPERIMENTAL

All chemicals and solvents were obtained from SD Fine Chem Ltd. (Mumbai, India) and used without further purification. The reaction progress was tracked using thin-layer chromatography on silica gel 60 F_{254} coated aluminum plates (0.5 mm; Merck, Germany). Melting points were determined with a MEL-TEMP Model 1202 apparatus. Infrared spectra were collected using a Shimadzu IR Tracer-100 spectrometer with KBr pellet method. Proton (^{1}H) and carbon (^{13}C) NMR spectra (400 MHz) were recorded on a Varian NMR spectrometer, using tetramethylsilane as the internal standard and chemical shifts expressed in δ (ppm). Mass spectral analyses were performed using an Agilent 7000-3Q triple quadrupole system operating in electron-impact mode at 70 eV.

Synthetic procedure

2-(6-Methyl-2-tolyl-imidazopyridin-3-yl)acetic acid (1): A solution of 2-(6-methyl-2-tolyl-imidazopyridin-3-yl)acetonitrile (1.5 g) in methanol (20 mL) was treated with aqueous KOH (0.161 g in 10 mL water) and refluxed with stirring for 2 h. Upon completion of the hydrolysis, the solvent was removed under vaccum and the resultant mixture was added to crushed ice. Thereafter, HCl was added dropwise to the reaction mixture to acidify to yield the final product. The resulting solid was collected by filtration, washed with cold water and dried under vacuum to afford the target carboxylic acid derivative as an off-white solid (0.98 g, 71% yield).

Ethyl-2-(2-(6-methyl-2-tolyl imidazopyridin-3-yl)acetamido)thiazole-5-carboxylate (2): Compound **1** (1.0 g) was dissolved in dichloromethane (25 mL) and stirred in a round-bottom flask. O-(Benzotriazol-1-yl)-*N*,*N*,*N*′,*N*′-tetramethyluronium tetrafluoroborate (TBTU) (2.44 g) and triethylamine (1.09 mL) were then added one after the other, followed by ethyl 2-aminothiazole-5-carboxylate (0.773 g). The mixture was refluxed with continuous stirring for 3 h and the reaction progress was tracked by TLC. After completion, the solvent was removed under reduced pressure and the residue was extracted with ethyl acetate. The combined organic layers were washed sequentially with saturated Na_2CO_3 solution, water and brine, dried over anhydrous Na_2SO_4 and concentrated. The crude product was obtained as a solid (0.82 g, 48.2% yield).

2-(2-(6-Methyl-2-tolyl-imidazopyridin-3-yl)acetamido)-thiazole-5-carboxylic acid (3): Compound **2** (1.0 g) was dissolved in 30 mL of methanol, then 10 mL of aqueous NaOH solution was added. The mixture was stirred at room temperature for 1 h. Upon completion, the solvent was removed under reduced pressure and the residue was dissolved in water and washed with ethyl acetate, discarding the organic layer. The aqueous phase containing the sodium salt was acidified with conc. HCl to precipitate the product. The resulting solid was filtered, rinsed with cold water and dried under vacuum to obtain compound **3** as a solid (0.64 g, 67.36%).

General method for the synthesis of *N*-substituted benzyl-2-(2-(6-methyl-2-tolylimidazopyridin-3-yl)acetamido)thiazole-5-carboxamide (4a-j): Compound **3** (0.20 g) was dissolved in 20 mL of dichloromethane in a round-bottom flask. Under N_2 atmosphere, EDCI (0.32 g), HOBt (0.12 g) and diisopropylamine (0.145 mL) were added to the stirred solution and mixed for 5 min. Benzylamine was then added and the mixture was refluxed for 3 h while monitoring the reaction progress by TLC. After completion, the reaction mixture was extracted with ethyl acetate and the combined organic layers were washed sequentially with saturated Na_2CO_3 solution, water and brine. The organic layer was dried over anhydrous Na_2SO_4, concentrated under reduced pressure and the crude product was recrystallised from ethanol to yield the N-substituted benzylamide derivatives **4a-j** (**Scheme-I**).

***N*-Benzyl-2-(2-(6-methyl-2-(*p*-tolyl)imidazo[1,2-*a*]-pyridin-3-yl)acetamido)thiazol-5-carboxamide (4a):** Colourless solid; yield: 68%; m.p.: 149-152 ºC. UV (MeOH): λ_{max}: 257 nm; IR (KBr, ν_{max}, cm^{-1}): 3292 (N–H), 1688 (C=O, amide), 1537 (C=N, imidazopyridine), 1283 (C–N), 797 (C–S), 2924 (C–H), 1492 (C=C, Ar), 824–697 (Ar vibrations); ^{1}H NMR

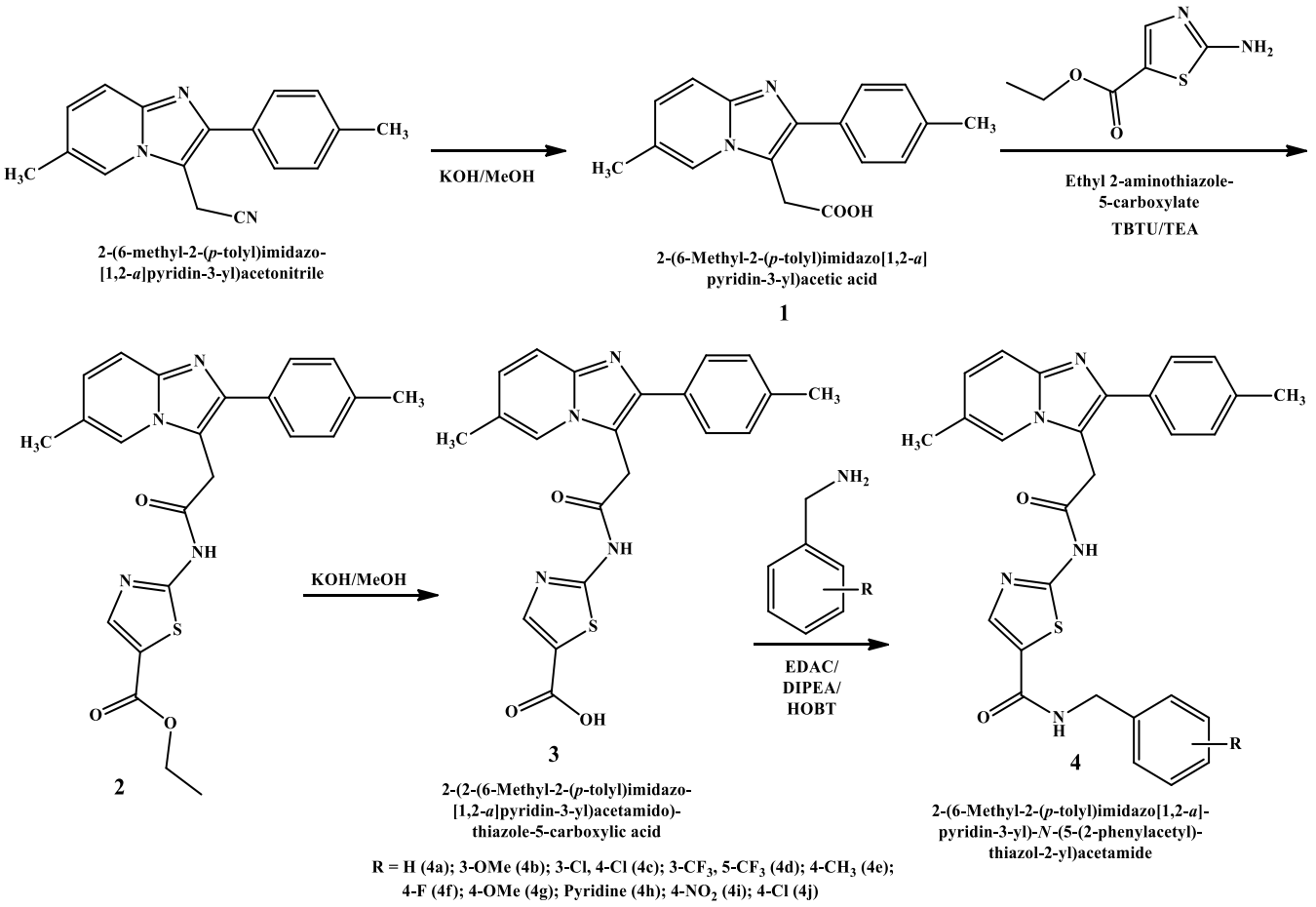

Scheme-I: Synthetic route of target molecules

(400 MHz, DMSO-d_6, δ ppm): 8.87, 8.85 (2H, 2×NH); 8.84, 8.29, 8.06, 7.69, 7.67, 7.51, 7.49, 7.38, 7.34, 7.32, 7.28, 7.25, 7.12 (m, 13H, Ar–H); 3.37 (m, 4H, 2×CH_2); 2.34, 2.31 (s, 6H, 2×CH_3); ^{13}C NMR (400 MHz, DMSO-d_6, δ ppm): 169.50, 161.11 (2×C=O), 163.53, 161.12, 154.60, 143.02, 142.69, 139.85, 139.63, 136.64, 131.82, 129.15, 128.57, 128.33, 127.70, 127.47, 127.31,127.00, 126.83, 126.15, 122.51, 120.91, 115.97, 114.40 (Ar-C, 22C), 44.37, 36.76 (CH_2), 20.85, 17.08 (CH_3). MS (ESI): *m/z* 495.87 [M^+]. m.f.: $C_{28}H_{25}N_5O_2S$.

***N*-(3-Methoxybenzyl)-2-(2-(6-methyl-2-(*p*-tolyl)imidazo[1,2-*a*]pyridin-3-yl)acetamido)thiazol-5-carboxamide (4b):** Colourless solid; yield: 60%; m.p.: 117-119 ºC. UV (MeOH): λ_{max}: 242 nm; IR (KBr, ν_{max}, cm^{-1}): 3444 (N–H), 1685 (C=O, amide), 1514 (C=N, imidazopyridine), 1616 (C=C, Ar), 1267 (C–N), 744 (C–S), 2924 (C–H), 995-453 (Ar vibrations); ^{1}H NMR (400 MHz, DMSO-d_6, δ ppm): 8.43, 8.35 (2H, 2×NH), 8.09, 8.00, 7.98, 7.84, 7.73, 7.71, 7.60, 7.58, 7.55, 7.53, 7.44, 6.82 (m, 12H, Ar-H), 4.47, 3.35 (m, 4H, 2×CH_2), 3.83 (s, 3H, OCH_3), 2.34, 2.33 (s, 6H, 2×CH_3); ^{13}C NMR (400 MHz, DMSO-d_6, δ ppm): 168.22, 162.39 (2×C=O), 162.39, 160.72, 159.36, 157.72, 144.54, 142.85, 142.56, 142.11, 141.02, 137.24,129.49, 129.34, 128.54, 127.85, 127.69, 127.34, 124.54, 122.71, 121.85, 119.44, 115.46, 109.66 (Ar-C, 22C), 55.03 (OCH_3), 42.27, 30.49 (2×CH_2), 20.85, 17.83 (2×CH_3); MS (ESI): *m/z* 526.39 [M^+]. m.f.: $C_{29}H_{27}N_5O_3S$. calcd. m.w.: 407.27.

***N*-(3,4-Dichlorobenzyl)-2-(2-(6-methyl-2-(*p*-tolyl)imidazo[1,2-*a*]pyridin-3-yl)acetamido)thiazol-5-carboxamide (4c):** Colourless solid; yield: 70%; m.p.: 157-159 ºC; UV (MeOH): λ_{max}: 242 nm; IR (KBr, ν_{max}, cm^{-1}): 3392 (N–H), 1629 (C=O, amide), 1545 (C=N, imidazopyridine), 1460 (C=C, Ar), 1261 (C–N), 744 (C–S), 2953 (C–H), 995-453 (Ar vibrations); ^{1}H NMR (400 MHz, DMSO-d_6, δ ppm): 8.67, 8.32 (2H, 2×NH), 7.89, 7.85, 7.79, 7.73, 7.71, 7.62, 7.61, 7.59, 7.57, 7.40, 7.33, 7.20 (m, 11H, Ar–H), 4.49, 4.36 (m, 4H, 2×CH_2), 2.34, 2.33 (s, 6H, 2×CH_3); ^{13}C NMR (400 MHz, DMSO-d_6, δ ppm): 168.95, 168.32 (2×C=O), 160.95, 157.74, 144.32, 142.76, 142.17, 140.88, 137.07, 131.00, 130.90, 130.54, 129.35, 129.29, 128.16, 127.64, 127.33, 124.52, 122.56, 121.58, 119.15, 118.11, 115.66, 109.63 (Ar-C, 22C), 41.32, 30.52 (CH_2), 20.84, 17.84 (CH_3). MS (ESI): *m/z* 564.31 [M^+]. m.f.: $C_{28}H_{23}Cl_2N_5O_2S$. calcd. m.w.: 564.49.

N-(3,5-*Bis*(trifluoromethyl)benzyl)-2-(2-(6-methyl-2-(*p*-tolyl)imidazo[1,2-*a*]pyridin-3-yl)acetamido)thiazol-5-carboxamide (4d): Colourless solid; yield: 62%; m.p.: 164-166 ºC. UV (MeOH): λ_{max}: 240 nm. IR (KBr, ν_{max}, cm^{-1}): 3416 (N–H), 1629 (C=O, amide), 1546 (C=N, imidazopyridine), 1492 (C=C, Ar), 1261 (C–N), 744 (C–S), 2924 (C–H), 898–457 (Ar vibrations); ^{1}H NMR (400 MHz, DMSO-d_6, δ ppm): 8.83, 8.79 (2H, 2×NH), 8.36, 8.08, 8.02, 8.00, 7.98, 7.87, 7.73, 7.61, 7.59, 7.57, 7.43 (m, 11H, Ar–H), 4.67, 3.32 (m, 4H, 2×CH_2), 2.39, 2.32 (s, 6H, 2×CH_3). ^{13}C NMR (400

MHz, DMSO-d_6, δ ppm): 168.35, 161.20 (2×C=O), 161.20, 157.82, 144.15, 143.29, 142.82, 142.28, 137.02, 131.09, 130.36, 130.03, 129.27, 128.15, 127.84, 127.64, 127.31, 124.76, 124.50, 122.53, 121.51, 119.14, 115.71, 109.63 (Ar-C, 22C), 124.75, 124.49 (2×CF_3), 41.73, 30.55 (CH_2), 20.81, 17.82 (CH_3); MS (ESI): *m/z* 632.90 [M^+]. m.f.: $C_{30}H_{23}F_6N_5O_2S$. calcd. m.w.: 631.59**.**

***N*-(4-Methylbenzyl)-2-(2-(6-methyl-2-(*p*-tolyl)imidazo-[1,2-*a*]pyridin-3yl)acetamido)thiazol-5-carboxamide (4e):** Colourless solid; yield: 62%; m.p.: 187-189 ºC; UV (MeOH): λ_{max}: 246 nm. IR (KBr, ν_{max}, cm^{-1}): 3416 (N–H), 1629 (C=O, amide), 1546 (C=N, imidazopyridine), 1492 (C=C, Ar), 1261 (C–N), 744 (C–S), 2924 (C–H), 898-457 (Ar vibrations). ^{1}H NMR (400 MHz, DMSO-d_6, δ ppm): 8.39, 8.37 (2H, 2×NH), 8.00, 7.73, 7.58, 7.54, 7.43, 7.41, 7.29, 7.27, 7.27, 7.22, 7.15 (m, 12H, Ar–H), 4.45, 4.39 (m, 4H, 2×CH_2), 2.38, 2.33, 2.28 (s, 9H, 3×CH_3); ^{13}C NMR (400 MHz, DMSO-d_6, δ ppm): 168.21, 160.60 (2×C=O), 160.60, 157.64, 144.55, 142.64, 141.97, 137.12, 136.34, 135.95, 130.82, 129.30, 128.90, 128.32, 127.82, 127.63, 127.29, 124.51, 122.61, 121.68, 119.15, 117.70, 115.55, 109.62 (Ar-C, 22C), 42.02, 30.48 (CH_2), 20.82, 20.69, 17.82 (CH_3); MS (ESI): *m/z* 510.79 [M^+]. m.f.: $C_{29}H_{27}N_5O_2S$. calcd. m.w.: 509.62.

***N*-(4-Fluorobenzyl)-2-(2-(6-methyl-2-(*p*-tolyl)imidaazo-[1,2-*a*]pyridin-3-yl)acetamido)thiazol-5-carboxamide (4f):** Colourless solid; yield: 65%; m.p.: 162-164 ºC; UV (MeOH): λ_{max}: 238 nm. IR (KBr, ν_{max}, cm^{-1}): 3421 (N–H), 1666 (C=O, amide), 1545 (C=N, imidazopyridine), 1569 (C=C, Ar), 1299 (C–N), 744 (C–S), 2924 (C–H), 943-418 (Ar vibrations). ^{1}H NMR (400 MHz, DMSO-d_6, δ ppm): 8.50, 8.37 (2H, 2×NH), 8.00-7.9,7.84, 7.74,7.55,7.42,7.36,7.30,7.30,7.16 (m, 12H, Ar–H), 4.47, 4.36 (m, 4H, 2×CH_2), 2.50, 2.34 (s, 6H, 2×CH_3). ^{13}C NMR (400 MHz, DMSO-d_6, δ ppm): 168.09, 162.56 (2×C=O), 162.36, 157.71, 142.84, 142.49, 142.08, 137.27, 129.34, 127.84, 127.69, 127.39, 124.56, 122.73, 122.61, 121.90, 119.18, 115.41, 115.20, 114.99, 113.67, 109.63 (Ar-C, 22C), 40.15, 30.45 (CH_2), 20.85, 17.82 (CH_3); MS (ESI): *m/z* 514.38 [M^+]. m.f.: $C_{28}H_{24}N_5FO_2S$. calcd. m.w.: 513.59.

***N*-(4-Methoxybenzyl)-2-(2-(6-methyl-2-(*p*-tolyl)imidazo-[1,2-*a*]pyridin-3-yl)acetamido)thiazol-5-carboxamide (4g):** Colourless solid; yield: 63%; m.p.: 183-185 ºC. UV (MeOH): λ_{max}: 240 nm. IR (KBr, ν_{max}, cm^{-1}): 3367 (N–H), 1680 (C=O, amide), 1550 (C=N, imidazopyridine), 1612 (C=C, Ar), 1249 (C–N), 744 (C–S), 2924 (C–H), 968–418 (Ar vibrations). ^{1}H NMR (400 MHz, DMSO-d_6, δ ppm): 8.37, 8.32 (2H, 2×NH), δ 6.89, 7.24, 7.27, 7.29, 7.30, 7.40, 7.53, 7.55, 7.57, 7.60, 7.62 and 8.00 (m, 12H, Ar–H), 4.42, 4.36 (m, 4H, 2×CH_2), 2.35, 2.33 (s, 6H, 2×CH_3), 3.80 (s, 3H, OCH_3); ^{13}C NMR (400 MHz, DMSO-d_6, δ ppm): 168.17, 162.53 (2×C=O), 162.34, 160.52, 158.29, 157.62, 144.57, 142.52, 137.21, 131.31, 129.31, 128.73, 128.55, 127.82, 127.65, 127.37, 124.54, 122.67, 119.15, 115.43, 113.76, 113.67, 109.61 (Ar-C, 22C), 55.08 (OCH_3), 41.73, 30.45 (CH_2), 20.83, 17.81 (CH_3); MS (ESI): *m/z* 497.42 [M^+]. m.f.: $C_{28}H_{27}N_5O_3S$. calcd. m.w.: 496.58.

***N*-(Pyridin-4-ylmethyl)-2-(2-(6-methyl-2-(*p*-tolyl)imi-dazo[1,2-*a*]pyridin-3-yl)acetamido)thiazol-5-carboxamide (4h):** Pale yellow solid; yield: 66%; m.p.: 184–186 ºC. UV (MeOH): λ_{max}: 224 nm; IR (KBr, ν_{max}, cm^{-1}): 3396 (N–H), 1660 (C=O, amide), 1552 (C=N, imidazopyridine), 1236 (C–N), 810–740 (Ar C–H), 2932 (C–H, CH_2/CH_3); ^{1}H NMR (400 MHz, DMSO-d_6, δ ppm): 8.66, 8.52 (2H, 2×NH), 8.31, 7.87, 7.73, 7.62, 7.60, 7.56, 7.31, 7.29, 7.27, 7.20, 7.18 (m, 12H, Ar–H), 4.45, 4.40 (m, 4H, 2×CH_2), 2.34, 2.29 (s, 6H, 2×CH_3); ^{13}C NMR (400 MHz, DMSO-d_6, δ ppm): 168.38, 161.14 (2×C=O), 161.14, 157.78, 149.53, 148.61, 144.31, 142.91, 142.41, 137.02,131.19, 129.29, 128.01, 127.66, 127.24, 124.48, 122.52, 122.15, 121.49, 119.13, 118.15, 115.77, 113.54, 109.68 (Ar-C, 22C), 41.46, 30.55 (CH_2), 20.84, 17.85 (CH_3); MS (ESI): *m/z* 497.42 [M^+]. m.f.: $C_{27}H_{24}N_6O_2S$. calcd. m.w.: 496.58.

2-(2-(6-Methyl-2-(*p*-tolyl)imidazo[1,2-*a*]pyridin-3-yl)-acetamido)-N-(4-nitrobenzyl)thiazol-5-carboxamide (4i): Colourless solid; yield: 61%; m.p.: 180-182 ºC; UV (MeOH): λ_{max}: 226 nm; IR (KBr, ν_{max}, cm^{-1}): 3431 (N–H), 1653 (C=O, amide), 1518 (C=N, imidazopyridine), 1614 (C=C, Ar), 1346 (NO_2), 1263 (C–N), 2926, 2862 (C–H, CH_2/CH_3). ^{1}H NMR (400 MHz, DMSO-d_6, δ ppm): 8.73, 8.48 (2H, 2×NH), 8.23, 8.21, 8.00, 7.87, 7.65, 7.60, 7.58, 7.56, 7.53, 7.43, 7.34 and 7.32 (m, 12H, Ar–H), 4.62, 4.43 (m, 4H, 2×CH_2), 2.37, 2.32 (s, 6H, 2×CH_3); ^{13}C NMR (400 MHz, DMSO-d_6, δ ppm): 167.98, 161.04 (2×C=O), 161.05, 157.72, 147.66, 146.48, 144.31, 142.84, 141.42, 139.75, 138.04, 130.40, 129.53, 128.89, 127.85, 127.37, 124.55, 123.58, 123.28, 123.16, 119.16, 118.25, 114.35, 109.65 (Ar-C, 22C); 41.98, 30.34 (CH_2), 20.88, 17.79 (CH_3); MS (ESI): *m/z* 541.41 [M^+]. m.f.: $C_{28}H_{24}N_6O_4S$. calcd. m.w.: 540.59.

***N*-(4-Chlorobenzyl)-2-(2-(6-methyl-2-(*p*-tolyl)imidazo-[1,2-*a*]pyridin-3-yl)acetamido)thiazol-5-carboxamide (4j):** Colourless solid; yield: 70%; m.p.: 138-140 ºC; UV (MeOH): λ_{max}: 248 nm. IR (KBr, ν_{max}, cm^{-1}): 3427 (N–H), 1654 (C=O, amide), 1552 (C=N, imidazopyridine), 1492 (C=C, arom.), 1267 (C–N), 750 (C–S), 2929 (C–H, CH_3); ^{1}H NMR (400 MHz, DMSO-d_6, δ ppm): 8.55, 8.32 (2H, 2×NH), 8.00, 7.84, 7.73, 7.61, 7.56, 7.53, 7.43, 7.39, 7.33, 7.29, 7.27, 7.23 (m, 12H, Ar–H), 4.48-4.39 (m, 4H, 2×CH_2), 2.39, 2.33 (s, 6H, 2×CH_3); ^{13}C NMR (400 MHz, DMSO-d_6, δ ppm): 168.23, 160.82 (2×C=O), 160.82, 157.68, 144.44, 142.82, 142.58, 141.84, 138.56, 137.19, 131.40, 130.70, 129.31, 129.13, 128.47, 128.29, 127.83, 127.66, 127.33, 124.52, 122.65, 121.79, 119.15, 117.92, 115.48, 113.67, 109.63 (Ar-C, 22C), 41.64, 30.48 (CH_2), 20.83, 17.82 (CH_3); MS (ESI): *m/z* 530.39 [M^+]. m.f.: $C_{28}H_{24}ClN_5O_2S$. calcd. m.w.: 530.04.

Molecular docking studies: Molecular docking studies targeted the human Akt serine/threonine kinase (PDB ID: 7NH5), a critical regulator in breast cancer cell proliferation and survival, utilizing AutoDock Vina. The Akt crystal structure was sourced from the Protein Data Bank and prepared by removing water molecules and ligands. Polar hydrogens were added and Gasteiger charges assigned *via* Autodocking Tools before exporting the protein in PDBQT format for docking simulations. Ligand molecules, were either drawn manually or retrieved from public chemical databases. Each ligand structure was optimised through energy minimisation using the MMFF94 force field in Avogadro software to obtain the most stable conformation. Rotatable bonds were defined, Gasteiger charges were assigned and the ligands were conv-

erted into PDBQT format for docking. The docking grid box was defined around the ATP-binding pocket of Akt, guided by the coordinates of the co-crystallised ligand and key active site residues reported in the literature. A configuration file was generated for each receptor–ligand system specifying receptor and ligand filenames, grid centre and dimensions, exhaustiveness and output file paths. Docking simulations were executed through the command-line interface of Auto Dock Vina, resulting in output files containing predicted binding poses and binding affinity (ΔG) values. The PyMOL and UCSF Chimera visualisation software were used to analyze the docked complexes, examining binding orientations, hydrogen bonds, hydrophobic interactions and pi–pi stacking. The binding energies and interaction profiles were used to assess the inhibitory potential of the selected ligands against Akt, providing molecular insights into their possible mechanism of action in breast cancer therapy [21].

MTT assay: The MCF-7 human breast adenocarcinoma cell line was sourced from the National Centre for Cell Science (NCCS), Pune, India. The cytotoxic effects of the synthesised compounds were evaluated using the MTT assay, a widely used quantitative colorimetric technique that measures mitochondrial metabolic activity. This assay relies on the enzymatic conversion of yellow tetrazolium dye 3-(4,5-dimethylthiazol-2-yl)-2,5-diphenyltetrazolium bromide (MTT) into insoluble purple formazan crystals by mitochondrial succinate dehydrogenase in living cells.

In this research, MCF-7 cells were grown in minimum essential medium (MEM) enriched with 10% fetal bovine serum (FBS) and antibiotics, maintained at 37 ºC in a humidified incubator with 5% CO_2. Following exposure to varying concentrations of the test compounds, MTT solution was added to each well and cells were incubated for 4 h to allow formazan formation. The resulting formazan crystals were dissolved in DMSO and absorbance was measured at 570 nm using a microplate reader. The absorbance intensity reflects the number of metabolically active cells, enabling assessment of cell viability and cytotoxic effects of the tested substances.

RESULTS AND DISCUSSION

The imidazo[1,2-*a*]pyridine-thiazole hybrid scaffold (**4a-j**) was synthesized by combining two pharmacophoric frameworks known for their effectiveness in kinase inhibition and anticancer drug development. The synthetic sequence shown in **Scheme-I** afforded a novel series of amide derivatives (**4a-j**), which were structurally characterised and evaluated systematically through molecular docking against Akt kinase (PDB 7NH5) and MTT cytotoxicity assay on MCF-7 breast carcinoma cells.

The synthetic methodology proceeded through four steps: (i) alkaline hydrolysis of the imidazo[1,2-*a*]pyridine nitrile to give the corresponding acetic acid; (ii) amide coupling with ethyl 2-aminothiazole-5-carboxylate *via* TBTU activation; (iii) ester hydrolysis; and (iv) coupling with various substituted benzylamines using EDCI/HOBt under nitrogen. Moderate yields (48-71%) were achieved across the series. The spectroscopic analysis including IR, ^{1}H NMR, ^{13}C NMR and MS verified the presence of key functional groups such as amide C=O (1650 cm^{-1}), imidazo C=N (~1550 cm^{-1}) and thiazole C–S (740 cm^{-1}), aligning with earlier findings on similar structures [22]. The data collectively validate the successful construction of dual-heterocyclic architectures suitable for the molecular docking and biological screening.

Cytotoxicity and structure activity relationship: MTT assays against MCF-7 cells revealed a clear SAR pattern. The nitrobenzyl analogue (**4j**) displayed the most significant cytotoxicity (IC_{50} = 35.85 μM), whereas methoxy- and methyl-substituted analogues (**4g**, **4e**, **4b**) showed moderate activity (IC_{50} = 60-95 μM) (Table-1). Strongly electron-withdrawing (CF_3, Cl, F) resulted in reduced activity (> 100 μM) (Fig. 1). These findings implied that an optimal balance between electron-withdrawing capacity and steric compatibility governs Akt binding. The improved potency of compound **4i** may be attributed to increased hydrogen-bond acceptor strength of the nitro group and enhanced π-π stacking interactions within the kinase pocket.

Molecular docking: Targeting Akt with heterocyclic scaffolds capable of mimicking ATP-binding interactions is therefore a rational approach to modulate this pathway. The current series was designed to exploit the imidazo[1,2-*a*]-pyridine nucleus for π–π stacking and the thiazole amide for hydrogen bonding within the ATP-binding cleft. When compared with the reference ligand borussertib, which has a docking score of -12.63 kcal/mol, the tested compounds show a range of affinities from -10.02 to 6.33 kcal/mol. Among compounds, **4f** has the best score (-10.02 kcal/mol), followed by **4i** (-9.66), **4g** (-9.66) and **4d** (–9.59), all indicating relatively strong predicted binding but still weaker than borussertib (Table-2). Other ligands such as **4h** (-9.43), **4a** (-9.29) and show solid but moderate reductions in predicted affinity compared to the reference. Meanwhile, **4c** (-8.66) and **4b** (-8.28) display moderate binding and the lowest scores belong to **4j** (-7.63) and **4e** (-6.33), marking them as the weakest predicted binders. So, none of the test compounds surpass standard borussertib, but **4f** is the closest in docking performance [23,24]. Analysis of interactions showed that all synthesised derivatives (**4a-j**) form crucial molecular contacts within the Akt binding site, featuring π–π stacking mainly with Trp80 and Tyr272, hydrophobic interactions with residues like Ile84, Val270/271, Leu210/264/295 and hydrogen bonds mostly with Thr82 and Asn53, frequently mediated by water molecules. Among the series, several compounds particularly **4f**, **4i** and **4g** displayed interaction patterns closely resembling the reference inhibitor borussertib, which exhibited the most

TABLE-1
In vitro CYTOTOXIC ACTIVITY OF IMIDAZOPYRIDINE–THIAZOLE DERIVATIVES (**4a-j**) AGAINST MCF-7 BREAST CANCER CELLS

Code	**4a**	**4b**	**4c**	**4d**	**4e**	**4f**	**4g**	**4h**	**4i**	**4j**	5-F-uracil
IC_{50} (μM)	>100	64.69	>100	>100	60.84	>100	95.13	>100	35.85	>100	6.42

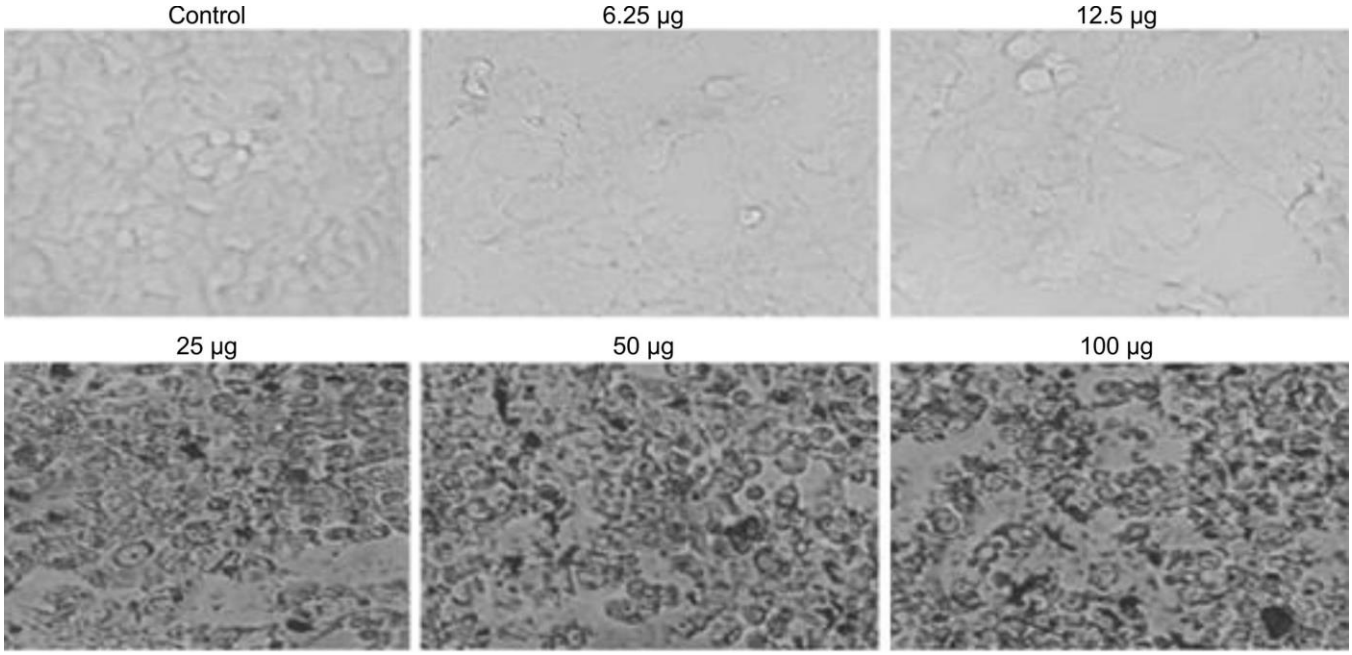

Fig. 1. Morphology of MCF-7 cells following treatment with compound **4i**

TABLE-2
MOLECULAR DOCKING SCORES OF IMIDAZOPYRIDINE–THIAZOLE DERIVATIVES (**4a-j**) AGAINST Akt KINASE (PDB: 7NH5)

Compd.	Docking score	π–π stacking	Hydrophobic interactions	Hydrogen-bond interactions
4a	-9.29802	TRP80, TYR272	ILE84; VAL270/271; LEU210/213/264/295; TYR263; TRP80	THR82; TYR272; ASN53 (H_2O); GLN79
4b	-8.28337	TRP80, TYR272	ILE84; VAL270/271; LEU210/213/264/295; TYR263	THR82; ASN53 (H_2O); ASP274
4c	-8.6683	TRP80	ILE84; VAL271; LEU210/264; ALA212	THR82; GLN79
4d	-9.59168	TRP80, TYR272	ILE84; VAL270; LEU213/295; TYR263	THR82; TYR272
4e	-6.33019	TRP80	ILE84; VAL270/271; LEU210/264	THR82; LYS268
4f	-10.024	TRP80, PHE225	ILE84; VAL270; LEU213/295	THR82; ASN53 (H_2O); SER205
4g	-9.66423	TRP80, TYR272	VAL270/271; LEU264/295; TYR263	THR82; GLN79
4h	-9.43012	TRP80	ILE84; VAL271; LEU210/213; CYS296	THR82; ASP274
4i	-9.66565	TRP80, TYR272	ILE84; ALA212; LEU210/295	THR82; ASN204
4j	-7.63098	TRP80, TYR272	VAL270/271; LEU213/264; TYR263	THR82; TYR272; ASN53 (H_2O)
Borussertib std.	-12.63	TRP80	LEU210, VAL270, VAL271, ILE290, LEU264, TYR263, TRP80, ILE84 and TYR18	Asn54, ARG 273 Asn53, VAL271

extensive and strongest interaction network, aligning with its superior docking score.

Conclusion

A novel series of imidazo[1,2-*a*]pyridine-thiazole hybrid amide compounds were efficiently synthesised, characterised and computationally assessed for their potential to inhibit Akt in breast cancer research. The study demonstrates that cytotoxic activity against MCF-7 cells is highly dependent on aromatic substitution, with the nitrobenzyl analogue showing the greatest potency. The optimal electronic effects combined with suitable steric compatibility are essential for effective Akt kinase interaction and enhanced anticancer activity. The molecular docking analysis revealed that several compounds exhibited favourable thermodynamic binding profiles, with **4f** emerging as the most promising test ligand based on its strongly negative docking energy. The predictive affinity of **4f** aligns well with previous reports highlighting imidazopyridine scaffolds as potent ATP-competitive inhibitors capable of engaging key hinge-region residues within the PI3K/Akt signalling pathway. Although none of the derivatives surpassed the reference inhibitor borussertib, the pronounced binding stability of **4f** suggests meaningful potential for modulation of Akt-driven oncogenic signaling. Finally, compound **4i** emerged as the most promising candidate based on its superior cytotoxic activity in cellular assays. Despite variations observed between docking and *in vitro* results, its overall biological performance supports effective target engagement. Therefore, compound **4i** warrants further investigation as a potential lead for the development of safe and effective anticancer agents.

ACKNOWLEDGEMENTS

The authors thank SRM Institute of Science and Technology for providing the facilities needed to carry out the research project.

CONFLICT OF INTEREST

The authors declare that there is no conflict of interests regarding the publication of this article.

DECLARATION OF AI-ASSISTED TECHNOLOGIES

During the preparation of this manuscript, the authors used an AI-assisted tool(s) to improve the language. The authors reviewed and edited the content and take full responsibility for the published work.

REFERENCES

1. S. Khatun, A. Singh, G.N. Bader and F.A. Sofi, *J. Biomol. Struct. Dyn.*, **40**, 14279 (2022); https://doi.org/10.1080/07391102.2021.1997818
2. E. Vitaku, D.T. Smith and J.T. Njardarson, *J. Med. Chem.*, **57**, 10257 (2014); https://doi.org/10.1021/jm501100b
3. M.E. Welsch, S.A. Snyder and B.R. Stockwell, *Curr. Opin. Chem. Biol.*, **14**, 347 (2010); https://doi.org/10.1016/j.cbpa.2010.02.018
4. N. Devi, R.K. Rawal and V. Singh, *Tetrahedron*, **71**, 183 (2015); https://doi.org/10.1016/j.tet.2014.10.032
5. M. Baumann and I.R. Baxendale, *Beilstein J. Org. Chem.*, **9**, 2265 (2013); https://doi.org/10.3762/bjoc.9.265
6. A. Ayati, S. Emami, A. Asadipour, A. Shafiee and A. Foroumadi, *Eur. J. Med. Chem.*, **97**, 699 (2015); https://doi.org/10.1016/j.ejmech.2015.04.015
7. P. Karegoudar, M.S. Karthikeyan, D.J. Prasad, M. Mahalinga, B.S. Holla and N.S. Kumari, *Eur. J. Med. Chem.*, **43**, 261 (2008); https://doi.org/10.1016/j.ejmech.2007.03.014
8. S.M. Gomha, H.A. Abdelhady, D.Z.H. Hassain, A.H. Abdelmonsef, M. El-Naggar, M.M. Elaasser and H.K. Mahmoud, *Drug Des. Devel. Ther.*, **15**, 659 (2021); https://doi.org/10.2147/DDDT.S291579
9. B.E. Evans, K.E. Rittle, M.G. Bock, R.M. DiPardo, R.M. Freidinger, W.L. Whitter, G.F. Lundell, D.F. Veber, P.S. Anderson, R.S. Chang, V.J. Lotti, D.J. Cerino, T.B. Chen, P.J. Kling, K.A. Kunkel, J.P. Springer and J. Hirshfield, *J. Med. Chem.*, **31**, 2235 (1988); https://doi.org/10.1021/jm00120a002
10. T.J. Ritchie and S.J. Macdonald, *Drug Discov. Today*, **14**, 1011 (2009); https://doi.org/10.1016/j.drudis.2009.07.014
11. N.A. Meanwell, *Chem. Res. Toxicol.*, **29**, 564 (2016); https://doi.org/10.1021/acs.chemrestox.6b00043
12. N. Devi, D. Singh, R. K. Rawal, J. Bariwal and V. Singh, *Curr. Top. Med. Chem.*, **16**, 2963 (2016); https://doi.org/10.2174/1568026616666160506145539
13. Z.A. Knight and K.M. Shokat, *Chem. Biol.*, **12**, 621 (2005); https://doi.org/10.1016/j.chembiol.2005.04.011
14. A. Kamal, G. Bharath Kumar, V. Lakshma Nayak, V.S. Reddy, A.B. Shaik, R. Rajender and M. Kashi Reddy, *MedChemComm*, **6**, 606 (2015); https://doi.org/10.1039/C4MD00400K
15. L.J. He, D.L. Yang, H.Y. Chen, J.H. Huang, Y.J. Zhang, H.X. Qin, J.L. Wang, D.Y. Tang and Z.Z. Chen, *OncoTargets Ther.*, **13**, 10111 (2020); https://doi.org/10.2147/OTT.S266752
16. S. Haider, M.S. Alam and H. Hamid, *Eur. J. Med. Chem.*, **92**, 156 (2015); https://doi.org/10.1016/j.ejmech.2014.12.035
17. S.I. Faggal, Y. El-Dash, A. Sonousi, A.M. Abdou and R.A. Hassan, *RSC Med. Chem.*, **15**, 4111 (2024); https://doi.org/10.1039/D4MD00462K
18. V.S.R. Avuthu, T.R. Allaka, N. Kushwaha and P.V.V.N. Kishore, *Chem. Biodivers.*, **22**, e202402470 (2025); https://doi.org/10.1002/cbdv.202402470
19. R. Morphy and Z. Rankovic, *J. Med. Chem.*, **48**, 6523 (2005); https://doi.org/10.1021/jm058225d
20. P. Liu, H. Cheng, T.M. Roberts and J.J. Zhao, *Nat. Rev. Drug Discov.*, **8**, 627 (2009); https://doi.org/10.1038/nrd2926
21. G.M. Morris, R. Huey, W. Lindstrom, M.F. Sanner, R.K. Belew, D.S. Goodsell and A.J. Olson, *J. Comput. Chem.*, **30**, 2785 (2009); https://doi.org/10.1002/jcc.21256
22. S.R. Shrimandilkar, A.G. Kadlag and D.D. Lokhande, *J. Mol. Struct.*, **1357**145267 (2026); https://doi.org/10.1016/j.molstruc.2026.145267
23. O. Trott and A.J. Olson, *J. Comput. Chem.*, **31**, 455 (2010); https://doi.org/10.1002/jcc.21334
24. G. Song, G. Ouyang and S. Bao, *J. Cell. Mol. Med.*, **9**, 59 (2005); https://doi.org/10.1111/j.1582-4934.2005.tb00337.x